The study of cerium containing phosphates with kosnarite structure in the context of nuclear waste disposal

Reactor Physics and Nuclear Materials

J.W. Keizers

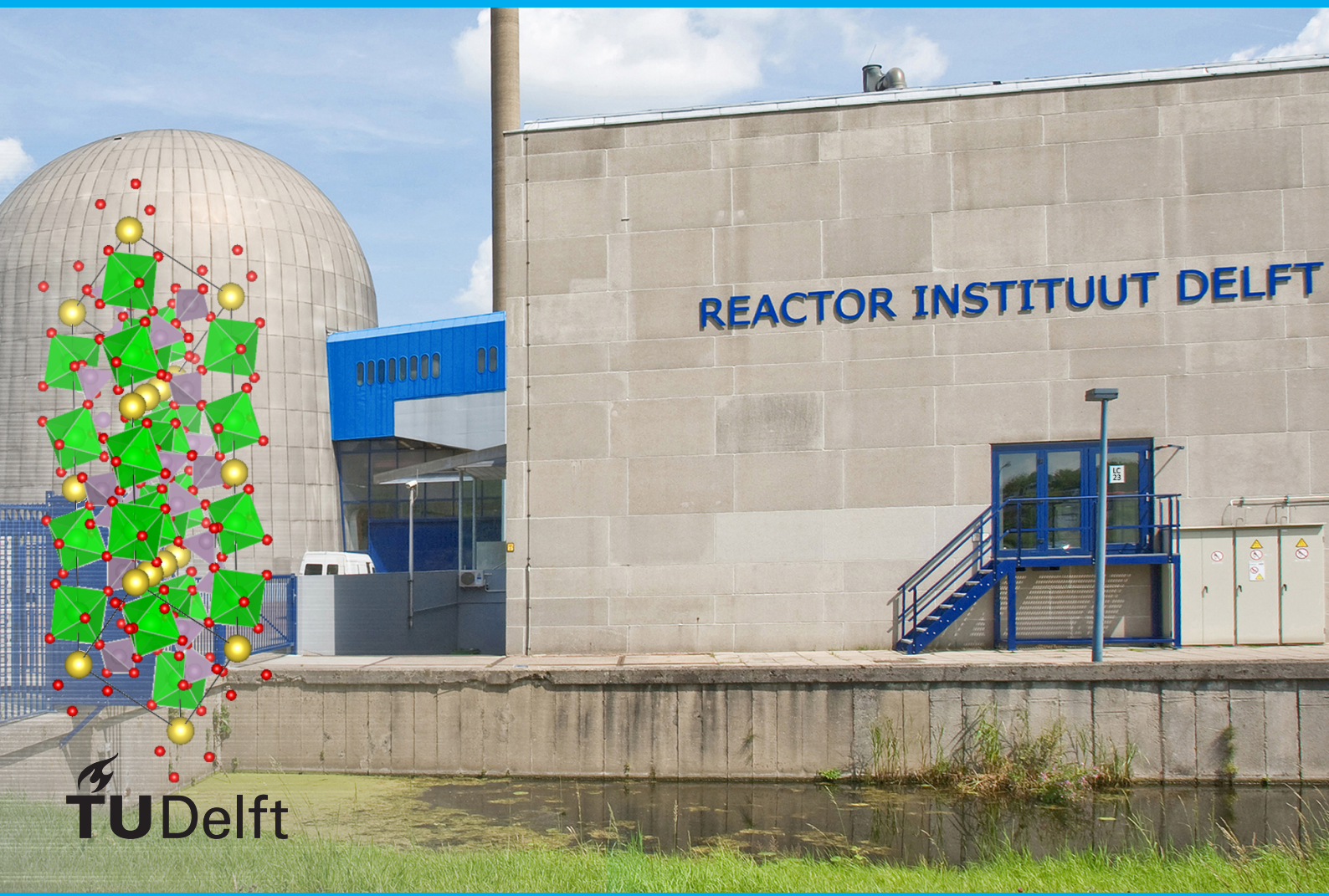

TU Delft

The study of cerium containing phosphates with kosnarite structure in the context of nuclear waste disposal

by

J.W. Keizers

to obtain the degree of
BSc Molecular Science and Technology
at the Delft University of Technology.

To be defended publicly on
Tuesday August 29, 2017 at 10:00 AM.

Faculty of Applied Sciences
Department of Radiation Science and Technology
Section of Reactor Physics and Nuclear Materials

Student number: 4385284
Email: J.W.Keizers@student.tudelft.nl
Project duration: February 6, 2017 – August 29, 2017
Thesis committee:

Dr. Denis Bykov,	TU Delft, supervisor
Dr. Erik Kelder,	TU Delft
Prof. Dr. Ir. Jan-Leen Kloosterman ,	TU Delft

An electronic version of this thesis is available at http://repository.tudelft.nl/.

TU Delft

Abstract

Safe storage of nuclear waste is still a big problem. Especially high-level waste (HLW) is problematic, as it is the source of the majority of the radioactivity and heat-emitting nuclides are a limiting factor for current storage options. Sodium zirconium phosphate (NZP) is a possible waste matrix. This work explores the possibility of using NZP-type ceramics for storage of actinides. Two series have been successfully synthesized using a solid-state synthesis at a final temperature of 800 °C, in which cerium (either trivalent or tetravalent) was used as a plutonium analogue. Cerium is also a close analogue to other actinides in the same oxidation state. The structural characteristics have been determined using X-ray diffraction (XRD). Scanning electron microscopy (SEM) was used to investigate the morphology of the particles and infrared-spectroscopy (IR) was used to examine the phosphate bonds of the NZP compounds. The space group transition from $R\bar{3}c$ to $R\bar{3}$ to $P\bar{3}c$ has been elucidated and was found to be similar for both series. Rietveld refinement showed profile parameter trends which were to be expected (a decrease and c increase with increased cerium substitution), SEM images showed a distinctive increase in particle size for the end-member $Ce_{0.33}Zr_2(PO_4)_3$, compared to the other compounds of the $Ce_{(x/3)}Na_{(1-x)}Zr_2(PO_4)_3$ series and IR-spectra proved the presence of the orthophosphate groups in the synthesized compounds.

Contents

Abstract iii

1 Introduction 1
- 1.1 Current storage . . . 1
- 1.2 Kosnarite . . . 2
  - 1.2.1 Crystal structure . . . 2
  - 1.2.2 Thermal stability . . . 3
  - 1.2.3 Isomorphism . . . 3
- 1.3 Cerium as Pu analogue . . . 4
  - 1.3.1 Variations from standard NZP model . . . 4
- 1.4 Goal . . . 4

2 Experimental 7
- 2.1 Synthesis . . . 7
  - 2.1.1 Cerium containing NZP-type ceramics . . . 7
  - 2.1.2 Materials . . . 7
  - 2.1.3 Solid-state synthesis . . . 7
- 2.2 Analysis . . . 8
  - 2.2.1 XRD . . . 8
  - 2.2.2 SEM . . . 10
  - 2.2.3 IR-spectroscopy . . . 10

3 Results and discussion 13
- 3.1 XRD . . . 13
  - 3.1.1 Space group . . . 13
  - 3.1.2 Refinement . . . 16
  - 3.1.3 Thermal stability . . . 20
- 3.2 SEM . . . 21
- 3.3 IR-spectroscopy . . . 23

4 Conclusion 27

A Acknowledgements 29

B Future research 31

Bibliography 33

1 Introduction

As with most technologies, nuclear energy also has its unique difficulties. Apart from potential nuclear disasters, possibly the biggest issue with current nuclear plants is the radioactive waste which is produced after the fuel rods have been depleted after the use in a nuclear reactor [1]. This waste can either be stored directly (open fuel cycle) or be reprocessed to recover the uranium and plutonium (closed fuel cycle). A closed fuel cycle is preferential in theory, as this is the right direction towards a circular economy, but the reprocessing also leads to further difficulties. The reprocessing yields four waste streams, of which high-level waste (HLW) accounts for more than 95% of all radioactivity, while it only makes up 3% of the entire waste volume [2]. This HLW consists of both beta and gamma emitting fission products and the minor actinides, long lived alpha emitting radio-nuclides such as Am-241, Am-243, Cm-245 and Np-237, as well as small amounts of unrecovered uranium and plutonium [3].

The total cumulative amount of spent fuel that will be generated by 2020 is estimated at 445,000 tons of heavy metal, of which approximately 73% will be stored [1]. Therefore, it is clear that good storage options are essential.

1.1. Current storage

Currently, two storage options are being used commercially. Either, wet storage of the spent fuel in large pools or dry storage in vaults or casks. Wet storage has been around for more than fifty years and has proven to be safe, although it was not originally the intention to use wet storage as a long-term storage option. Dry storage has been under development more recently and although the heat dissipation capabilities are less than those of wet storage, it is expected to be more cost efficient over time [1]. Especially with recent plans for geological repositories in many countries, interest is high to improve the dry storage technology.

When HLW is designated for dry storage it is currently most frequently vitrified. During this process it is melted together with borosilicate glass materials in order to incorporate the HLW into the structure of the glass [2]. The resulting glass melt is then stored in stainless steel containers. The containers must subsequently be cooled constantly as thermal stress and possible changes in the structure of the glass could otherwise result in a loss of integrity of the storage material [1]. This indicates that thermal stability is a limiting factor to this technology. This raises the question whether other materials might be a better option for long-term dry storage as it would be best to contain the HLW within a material, a waste matrix, which is inherently safe and exhibits great chemical stability, is thermally stable and is not affected by radiation from the stored radioactive compounds. Ceramics are an option worth exploring for problematic waste streams or specific waste streams, for example, long-lived wastes or strong heat-emitting wastes.

1.2. Kosnarite

When French researchers found the remains of an ancient natural nuclear reactor in Oklo, Gabon in 1972 this sparked the interest of several researchers, as the local phosphate-rich geological structures did a great job of containing the “spent fuel” ([2], [4]). Among other phosphates, sodium zirconium phosphate (NZP), based on the natural analogue kosnarite [5], attracts the attention of researchers around the world (e.g. USA, Russia, China), mainly as it possesses the ability to incorporate close to every element (including almost all 42 long-lived nuclides typically present in nuclear waste) into its structure without altering the characteristics of the materials ([6], [7]). Furthermore, the characteristics of NZP make it favourable to use for dry storage as the thermal expansion is low (near zero) [6] and it is more resistant to corrosion by geological fluids than borosilicate glass [2]. An additional benefit is that the zirconium and phosphate are already present in the current fuel cycle, which could be another step forward to a circular economy. Furthermore, a sodium source is also available, as a sodium nitrate solution stream is generated in the reprocessing plant as a result of nitric acid neutralization during the process [8].

1.2.1. Crystal structure

The crystal structure of NZP was first elucidated by Hagman et al. in 1962. They discovered that NZP has space group $R\bar{3}c$ and consists of hexagonal unit cells [9]. The crystals are constituted by ZrO_6 octahedra and PO_4 tetrahedra. These structural blocks are connected at the corners to form a three-dimensional network. The unit cell of the NZP structure has such properties that $a=b\neq c$ and $\alpha=\beta=90°$, with $\gamma=120°$, as shown in Figure 1.1. The sodium atoms are octahedrally surrounded by the oxygen atoms as visualized in Figure 1.2.

To generalize the NZP type structure, it can be described by the crystal chemical formula $(M1)(M2)[L_2(PO_4)_3]$. The M1 and M2 positions can accomodate various cations, which will fill the spaces within the structural framework created by the cations in the L position and the phosphate groups ([10], [11]).

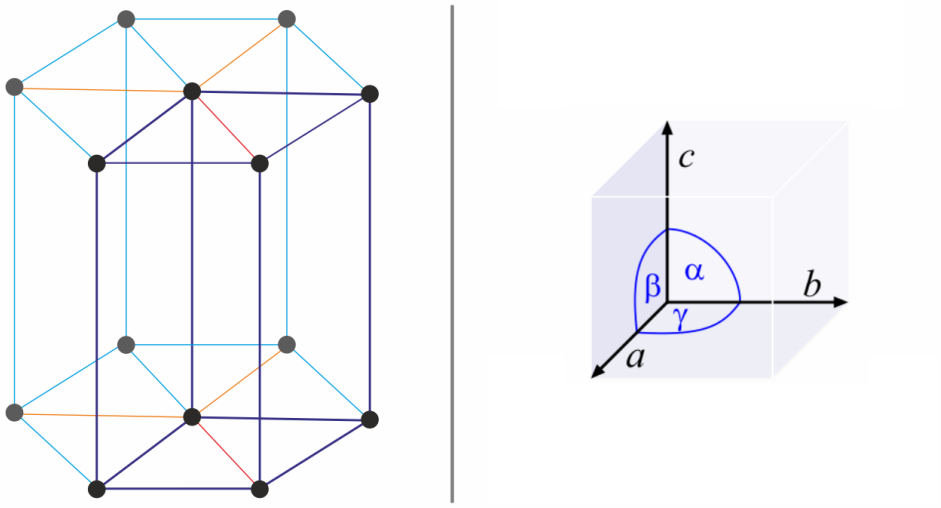

Figure 1.1: Example of a hexagonal unit cell (purple lines). The image on the right provides clarification on the angles (α, β and γ) and ordering of the unit cell parameters (a, b and c).

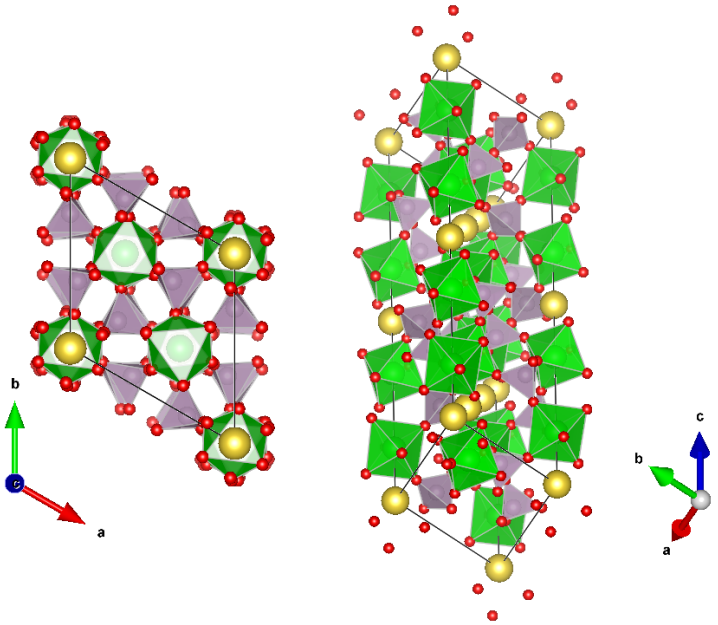

Figure 1.2: Two renderings from different angles as produced by VESTA [12] of the NZP unit cell. The green polyhedra represent the ZrO_6 octahedra with a zirconium atom in its center while the purple ones represent the PO_4 tetrahedra. Oxygen and sodium atoms are respectively shown in red and yellow.

1.2.2. Thermal stability

One of the most desirable properties of NZP materials is the thermal stability. This includes a near zero thermal expansion, high melting point and low thermal-conductivity ([11], [13]). The linear thermal expansion coefficient of α_{av}= 6 $\times 10^{-6}$ K^{-1} is similar to those of the best low-expansion ceramics, such as cordierite and zircon ([13], [14]). While some glasses, like silica glass, also show low thermal expansion, the thermal stability of typically used borosilicate glass diminishes considerably above 550 °C [15]. For NZP no stability problems should arise until at least 1000 °C, but a decomposition temperature as high as 1700 °C has also been documented ([16], [17]).

These properties make NZP an attractive potential host structure for the immobilization of nuclear waste, as the structure will not be compromised by the heat emission of radioactive nuclides in the matrix.

1.2.3. Isomorphism

Theoretically, allowing up to five different cationic species to take either the M1, M2 or L position, 212 different formula types are possible for the general NZP structure type. About half of the already characterized formula types show the three-dimensional $L_2(PO_4)_3$ framework where L is octahedrally coordinated, as previously described [13]. This indicates that it should be possible to accommodate a variety of different cations present in nuclear waste.

The coordination number for the M1 and L sites is 6, whereas the M2 site has a coordination number of 8 ([18], [19], [20]). For substitution to be possible, the cation has to be able to coordinate in the structure without distorting the framework. As an effect the usually unpopulated M2 position can only hold sodium and potassium ions, whereas M1 is suitable for larger cations as well [6]. In $NaZr_2(PO_4)_3$ only the M1 sites are occupied by the sodium cations [11]. Cations with the possibility of being substituted into the M1, M2 or L site have been identified and are presented in Table 1.1.

Within this research only M1 substitution is to be expected following the Goldschmidt rules for ionic substitution, as the difference in ionic radii between Zr^{4+} and Ce^{3+} or Ce^{4+} far ex-

ceeds 15% [21], although Japanese research indicates that minor substitution could still be found considering the ionic radii of cerium in both oxidation states [22]. The substitution of Ce^{3+} will certainly be close to zero for the L position.

Table 1.1: Overview of the possible substitutions made within the M1, M2 and L sites of NZP [23].

Site	*Cation*
M1	Li, Na, K, Rb, Cs, Cu, Ag Mg, Ca, Sr, Ba, Mn, Co, Ni, Cu, Zn, Cd Sc, Fe, Bi, Ce-Lu Zr, Hf, Np, Pu
M2	Na, K
L	Na, K Mg, Mn, Zn, Ni, Cu, Co Al, Sc, Cr, Fe, Ga, Y, In, Gd, Tb, Dy, Er, Yb Ti, Ge, Zr, Mo, Sn, Hf, U, Np, Pu V, Nb, Sb, Ta

1.3. Cerium as Pu analogue

As it would be costly and not possible with our current facilities to work with actual radioactive waste in terms of safety, an analogue for plutonium was used in this work. Cerium has been selected for this purpose for multiple reasons.

Firstly, cerium oxide has the same fluorite structure as plutonium oxide, indicating similar crystallographic features [24]. Secondly, the oxidation states of cerium, either 3+ or 4+, are also present in plutonium. Additionally, the ionic radii are similar ($r_{ionic,\ Pu(III)}$= 1.00Å, $r_{ionic,\ Ce(III)}$= 1.01Å/$r_{ionic,\ Pu(IV)}$= 0.86Å, $r_{ionic,\ Ce(IV)}$= 0.87Å[25]). Lastly, cerium has been used before as an analogue for plutonium, due to similarity in redox properties [2]. These three factors make cerium a good proxy for plutonium [26].

Although most plutonium is removed from the spent fuel during reprocessing, the choice for cerium, can be justified for multiple reasons. Firstly, cerium is also a close analogue to other actinides, which are abundant in HLW, in the equivalent oxidation state ([24], [26]). Secondly, it supports fundamental plutonium chemistry research. Thirdly, although the USA withdrew from the Surplus Plutonium Disposition Program, research aimed at storing Cold War plutonium, in 2002 [27], the scientific interest has not yet subsided.

1.3.1. Variations from standard NZP model

The crystal structure of $Ce_{0.33}Zr_2(PO_4)_3$ has been characterized by Bykov et al. and deviations from the $NaZr_2(PO_4)_3$ system have been documented. The complete substitution of sodium for the trivalent cerium caused a shift in space group from $R\bar{3}c$ to $P\bar{3}c$ [28]. Characterization has only been done on the end-member, so it is not yet known at which loading of cerium this transition will occur and through which mechanism. This transition is interesting to examine, as knowing the intermediary structures and structural changes is important for assessing the properties of the material.

1.4. Goal

The goal of the current research is to synthesize and characterize the entire series (x = 0.0-1.0 in steps of 0.1) for both trivalent ($Ce_{(x/3)}Na_{(1-x)}Zr_2(PO_4)_3$) and tetravalent ($Ce_{(x/4)}Na_{(1-x)}Zr_2(PO_4)_3$) cerium doped NZP in order to attain a better understanding of the possibilities for the utilization of this material in the context of nuclear waste storage. Characterization is done by XRD, SEM and IR-spectroscopy.

2

Experimental

2.1. Synthesis

2.1.1. Cerium containing NZP-type ceramics

To obtain information on the behaviour of cerium containing NZP-type ceramics two series of solid solutions have been synthesized. The two series, for trivalent cerium and tetravalent cerium respectively can be generalized by the following formulas:

1. $Ce_{(x/3)}Na_{(1-x)}Zr_2(PO_4)_3$
2. $Ce_{(x/4)}Na_{(1-x)}Zr_2(PO_4)_3$

The x in both series ranges between 0 and 1, with a step size of 0.1. This results in a total of 21 samples, which have all been similarly prepared as described in Section 2.1.3.

2.1.2. Materials

In the synthesis process of the two series of NZP materials, sodium nitrate, zirconyl chloride and a phosphoric acid solution in water (85 wt.%) have been used. For the trivalent series, cerium(III)nitrate, was used as a cerium source, whereas ceric ammonium nitrate has been used for the tetravalent series. The concentrated phosphoric acid solution of 85 wt.% was diluted to 1M, prior to synthesis. An overview of the materials used, can be found in Table 2.1.

Table 2.1: Summary of the chemicals used during synthesis.

Name	***Formula***	***Purity (%)***	***Supplier***
Sodium nitrate	$NaNO_3$	≥99.0	J.T. Baker
Zirconyl chloride	$ZrOCl_2{\cdot}8\ H_2O$	≥99.0	Fluka
Zirconyl chloride	$ZrOCl_2{\cdot}8\ H_2O$	≥99.5	Sigma-Aldrich
Cerium nitrate	$Ce(NO_3)_3{\cdot}6\ H_2O$	≥98.5	Merck
Ceric ammonium nitrate	$(NH_4)_2Ce(NO_3)_6$	≥99.0	Merck
Phosphoric acid	H_3PO_4	-	Sigma-Aldrich

2.1.3. Solid-state synthesis

A sol-gel synthesis approach been found to produce crystalline NZP by ([29], [30]). In this study a similar method has been used in combination with a solid-state reaction, which has also been found to be effective [31]. Precaution was to be taken, to ensure that the tetravalent cerium would not get reduced by an aqueous environment. To guarantee this, a precursor was made in order to eliminate any H_2O, preventing the water molecules from coming into contact with Ce^{4+}. A summary of the general procedure for both series can be found in Figure 2.2.

Precursor
To produce the precursor, $Zr(HPO_4)_2 \cdot H_2O$, a stoichiometric amount of phosphoric acid solution was added to a weighed amount of zirconyl chloride powder in a glass beaker. Subsequently, the liquid was stirred until the zirconyl chloride powder was completely incorporated in the suspension and a gel was formed. Finally, the gel was dried on a hot plate of approximately 90 °C until all the liquid had been evaporated. During this process zirconium hydro orthophosphate is formed according to the reaction presented in Figure 2.1 [32].

After the drying process, the precursor is completely white. It is very brittle and can be finely ground in an agate mortar with little force.

$$ZrOCl_2 + 2H_3PO_4 \rightarrow Zr(HPO_4)_2 \bullet H_2O + 2HCl$$

Figure 2.1: Reaction formula for the synthesis of the precursor.

Solid-state reaction
Firstly, the precursor and the necessary cerium and sodium compound were weighed and mixed in an agate mortar, in which they were ground for ten minutes to both homogenize the mixture of powders and increase the surface area of the powder particles, to improve the reactivity of the mixture.

Secondly, the powder was heated in a furnace to produce a phase pure crystalline product. Heating was performed in two heat treatment steps of 24 hours, at 600 °C and at 800 °C (heating rate of 5 °C/minute), with intermittent grinding of 10 minutes to improve crystallinity of the final solid solution.

Both heat treatment for the tetravalent series have been done in a furnace under oxygen atmosphere to prevent the reduction of Ce^{4+} to Ce^{3+} in the sample. Care has been taken to ensure that the air inside the furnace had been replaced with oxygen before starting the heat treatment by flowing oxygen through the furnace for two hours prior to heating. The heat treatment scheme is presented in Figure 2.3

2.2. Analysis
In the following four sections the different methods of analysis are introduced and the method of sample preparation is specified where relevant.

2.2.1. XRD
To determine the crystal structure and the phase purity of the synthesized compounds, X-ray diffraction (XRD) was used. Predominantly, the instrument X'pert Pro MPD DY2977 has been used with a copper X-ray tube (λ_1=1.54056 Å), λ_2=1.54439 Å) in the 2θ range of 5°-120°. To check the phase purity of the tetravalent series, measurements were initially done using a cobalt X-ray tube (λ=1.79 Å) in the 2θ range of 10°-50°.

This technique, based on Bragg's law (Equation 2.1), is used to measure reflections created by the crystal lattice structure. Based on the structure and the angle of reflection as predicted by Bragg's law, a XRD measurement can subsequently be used to determine crystallographic parameters [33].

$$n\lambda = 2d \sin(\theta) \tag{2.1}$$

In Bragg's law n is an integer (1, 2, 3...), λ is the wavelength of the X-rays which are used (nm), d represents the spacing between the crystal lattice planes (nm) and θ is the angle of incidence of the X-rays relative to the surface of the sample (°).

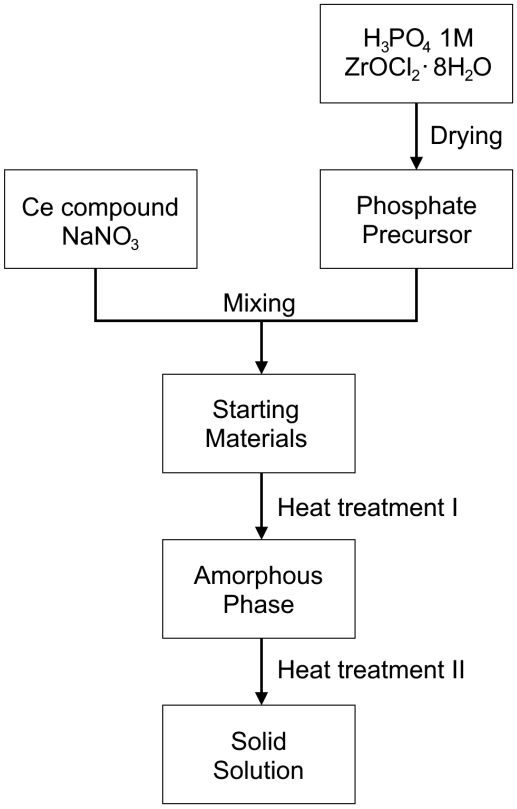

Figure 2.2: Schematic presentation of the synthesis route followed. The cerium containing compound was different for both series. For the $Ce_{(x/3)}Na_{(1-x)}Zr_2(PO_4)_3$ series $Ce(NO_3)_3 \cdot 6\ H_2O$ was used, for the $Ce_{(x/4)}Na_{(1-x)}Zr_2(PO_4)_3$ series $(NH_4)_2Ce(NO_3)_6$ was used.

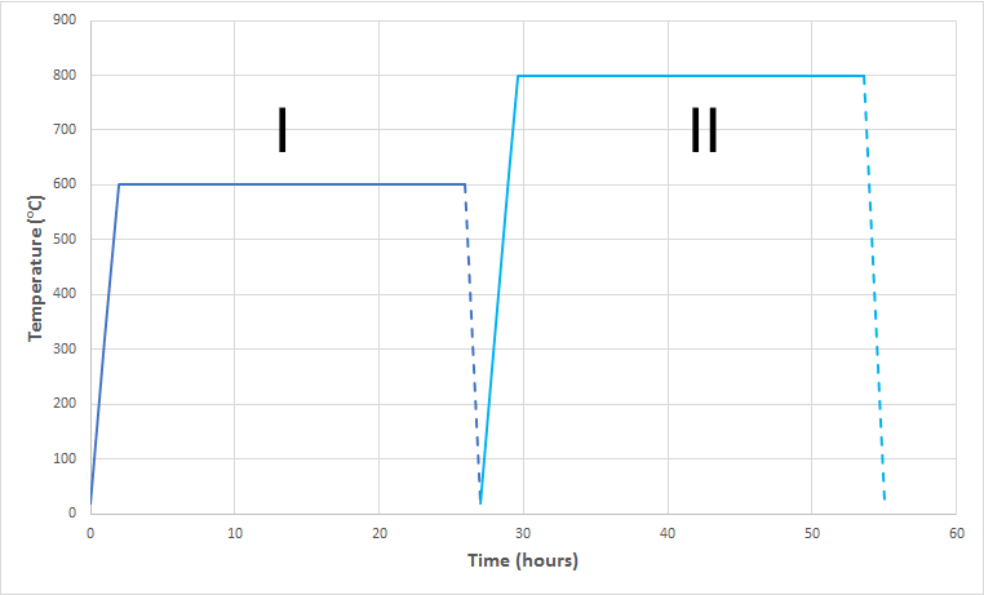

Figure 2.3: Schematic presentation of the heat treatments. Note that the cooling down, shown as dotted lines, is not as fast in reality. The heating rate is 5 °C/minute and the dwelling time is 24 hours.

For collection of data suitable for Rietveld refinement the measurement time was 2 hours, while spinning the sample (15 rpm).

Rietveld refinement

While the XRD measurements provide useful insight on the structure of a compound, especially when paired with database software such as X'pert Highscore [34], it cannot directly be used to determine lattice parameters. Rietveld refinement does give this opportunity. The principal of this refinement is a mathematical least-squares approach to match a profile fitting to the experimental data. In this research FullProf [35] has been used to determine the structural parameters. This method of refinement requires an initial structural model close to the actual structure to begin the refinement process. To this extent structural data for $NaZr_2(PO_4)_3$ [9], $Ca_{0.25}Sr_{0.25}Zr_2(PO_4)_3$ [36] and $Ce_{0.33}Zr_2(PO_4)_3$ [28] were used.

2.2.2. SEM

Scanning electron microscope (SEM) pictures were taken from a selection of samples in order to see whether any clear visual deviations are apparent in morphology between the compounds within a series. Using SEM, a high magnification can be achieved by analysis of the signals created by electrons which impinge on the analyte [37].

Small amounts of the powder were prepared on carbon tape and loaded in the scanning electron microscope (JEOL JSM-IT 100) without any additional coating. Roughly the same magnification, between 700 and 900 times, has been used in every picture to ease the qualitative comparison between the samples.

2.2.3. IR-spectroscopy

In addition to XRD, infrared (IR) spectroscopy was used for structural elucidation of the synthesized compounds. IR-spectroscopy, based on the various vibrations of the atoms within a molecule [38], can be used to aid the structural determination by clarification of the change in phosphate bond orientation and their vibrational modes within a series of compounds ([39], [40]).

To prepare a sample suited for IR-spectroscopy, pellets of 0.60 grams were pressed in a hydraulic press at 10 tons using a die (Figure 2.4). To achieve a well-defined spectrum without over-saturation of the IR signal the powders were mixed with potassium bromide (Merck, ≥99.5%). The ideal ratio of KBr to sample has been previously found to be 99.9% of KBr to 0.1% of the NZP compound [17]. The Shimadzu FTIR-8300 was used for IR-spectroscopy measurement in the range of 200 to 4000 cm^{-1}.

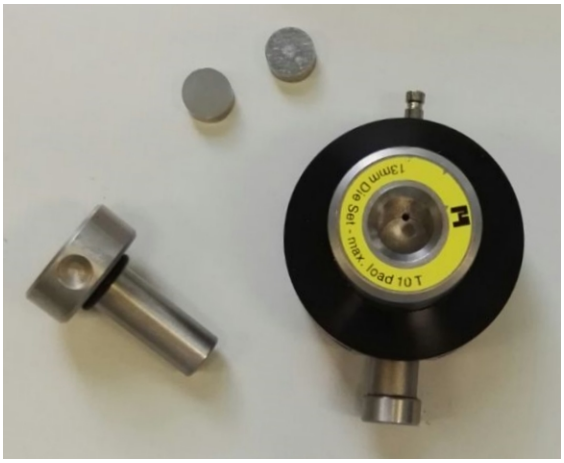

Figure 2.4: The die used to prepare the pellets for IR-spectroscopy.

3

Results and discussion

3.1. XRD

3.1.1. Space group

The entire series containing cerium with expected oxidation state 3+ ($Ce_{(x/3)}Na_{(1-x)}Zr_2(PO_4)_3$) has been measured for two hours as described in Section 2.2.1. The XRD results of the trivalent series are given in Figure 3.1. The full results of the quick scan and the full-range measurement of the $Ce_{(x/4)}Na_{(1-x)}Zr_2(PO_4)_3$ series can be found in Figures 3.2 and 3.3.

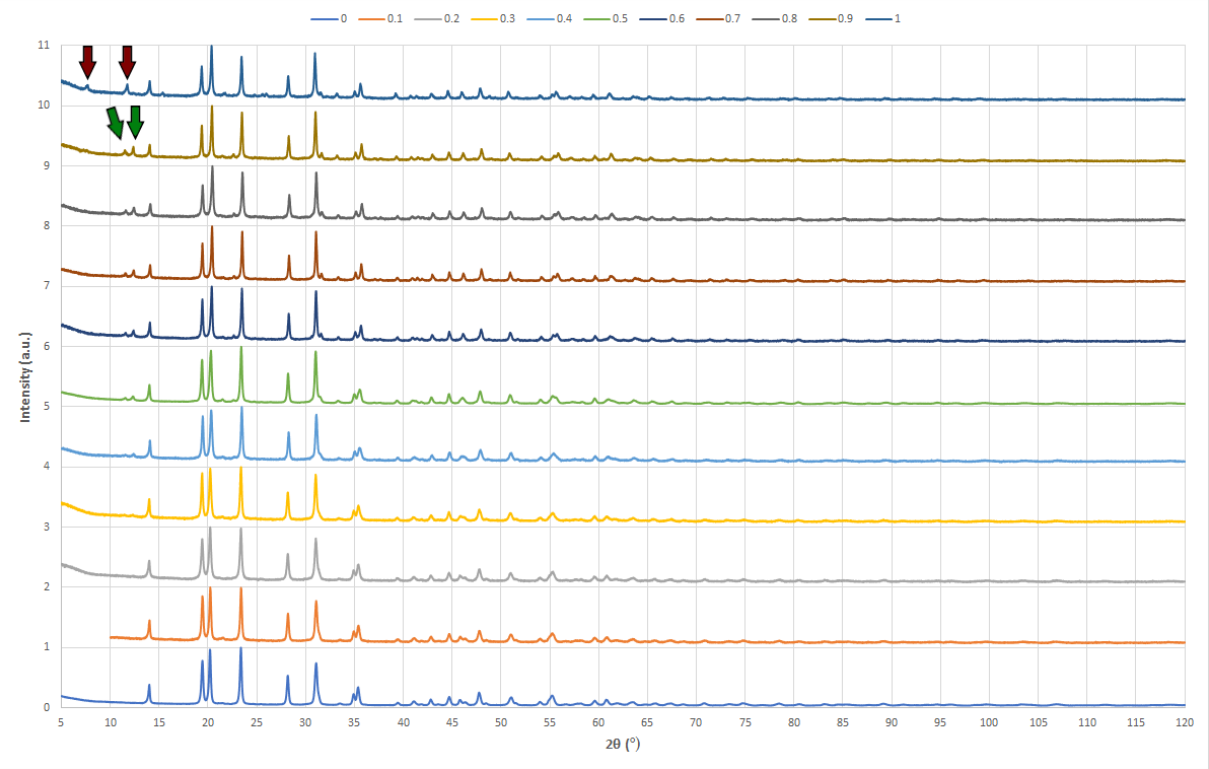

Figure 3.1: Diffractograms of the $Ce_{(x/3)}Na_{(1-x)}Zr_2(PO_4)_3$ series (copper X-ray tube). Red arrows indicate the reflections specific to the $P\bar{3}c$ space group, green arrows indicate the reflections specific to the $R\bar{3}$ space group. A lack of the indicated reflections indicates a $R\bar{3}c$ space group.

Three distinct pattern types can be identified from the XRD results, based on the positions of the reflections present in the diffractograms. Additionally, reflections caused by an admixture can be seen. A minor amount of a secondary, ZrP_2O_7, phase is visible in various samples. This phase is responsible for the low-intensity reflections at 21.5 °2θ.

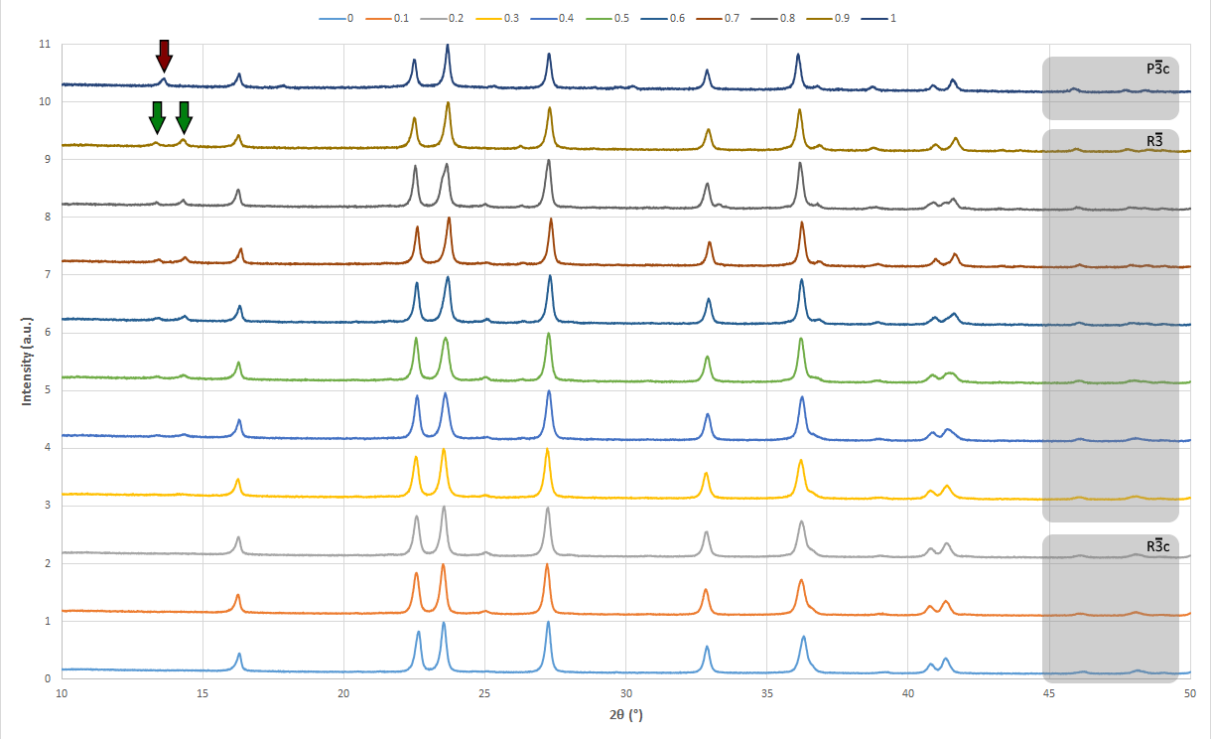

Figure 3.2: Diffractograms of the $Ce_{(x/4)}Na_{(1-x)}Zr_2(PO_4)_3$ series (cobalt X-ray tube). Grey bars indicate the different pattern areas, from bottom to top, R3̄c, R3̄ and P3̄c

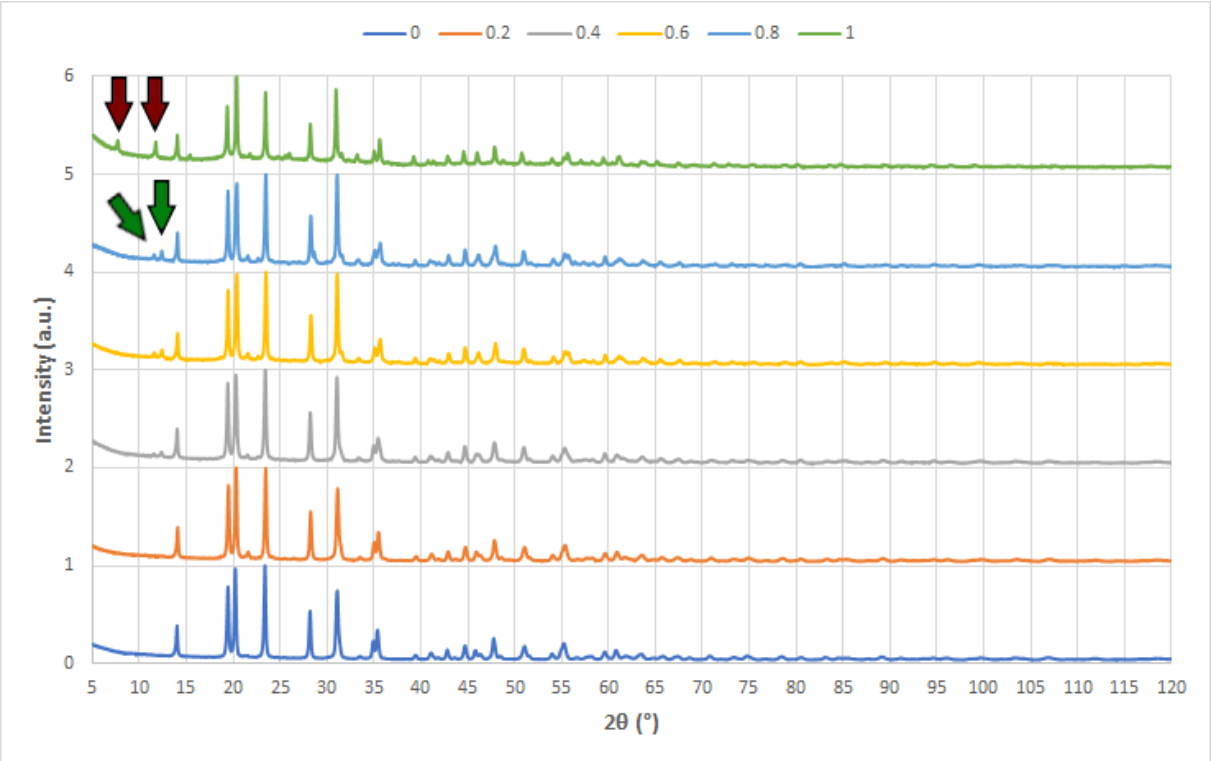

Figure 3.3: Diffractograms of the $Ce_{(x/4)}Na_{(1-x)}Zr_2(PO_4)_3$ series (copper X-ray tube). Red arrows indicate the reflections specific to the P3̄c space group, green arrows indicate the reflections specific to the R3̄ space group. A lack of the indicated reflections indicates a R3̄c space group.

As more sodium is substituted for cerium a reduction of symmetry introduces additional reflections in comparison to the pattern of pure $NaZr_2(PO_4)_3$ ($x = 0$) at 11.6°2θ and 12.4°2θ. These reflections are contraindicative of the R$\bar{3}$c space group, as the c-glide plane would result in extinction of the reflection at these angles [41]. After the quick scan had been performed and analyzed for the $Ce_{(x/4)}Na_{(1-x)}Zr_2(PO_4)_3$ series, the similarity with the $Ce_{(x/3)}Na_{(1-x)}Zr_2(PO_4)_3$ series was striking. Therefore, only selected samples for the tetravalent series have been measured in the full 2θ range.

This reduction of symmetry is documented for various compounds, such as $Cd_{0.5}Zr_2(PO_4)_3$ and $Ca_{0.25}Sr_{0.25}Zr_2(PO_4)_3$, in which the overall structure type show similarity with $NaZr_2(PO_4)_3$, with a decrease in M1 position occupation ([28], [36]). In these compounds the space group is R$\bar{3}$. Profile fitting done with Rietveld refinement, part of which can be found in Figures 3.5, 3.6 and 3.7, has proven that this space group is also apparent in both series investigated. The resulting structure fragments were rendered in VESTA (Figure 3.9), which shows the rearrangement of the polyhedra.

Initially, the XRD results were not conclusive on the existence of the two reflections in the 11.5°2θ to 12.5°2θ range for $Ce_{0.1}Na_{0.7}Zr_2(PO_4)_3$ ($x = 0.3$, trivalent series), so an additional longer scan of twenty minutes was done specifically in this region. This result (Figure 3.4) shows that this compound is the first to exhibit space group R$\bar{3}$.

Both end-members of the two series crystallize in the P$\bar{3}$c space group ([28], [42]). In the diffractogram this shift is most easily detected by the reflection around 7.7°2θ, which cannot be found in the diffractograms of compounds in space group R$\bar{3}$c or R$\bar{3}$. The space groups of all members of both series are summarized in Table 3.1.

Table 3.1: Synthesized compounds and their respective space group as determined by XRD profile fitting. Additionally, the M1 positions occupation is noted for both series.

	Ce^{3+}		Ce^{4+}	
x	Space group	M1 occupation (%)	Space group	M1 occupation (%)
0	R$\bar{3}$c	100	R$\bar{3}$c	100
0.1	R$\bar{3}$c	93.3	R$\bar{3}$c	92.5
0.2	R$\bar{3}$c	86.7	R$\bar{3}$c	85.0
0.3	R$\bar{3}$	80.0	R$\bar{3}$	77.5
0.4	R$\bar{3}$	73.3	R$\bar{3}$	70.0
0.5	R$\bar{3}$	66.7	R$\bar{3}$	62.5
0.6	R$\bar{3}$	60.0	R$\bar{3}$	55.0
0.7	R$\bar{3}$	53.3	R$\bar{3}$	47.5
0.8	R$\bar{3}$	46.7	R$\bar{3}$	40.0
0.9	R$\bar{3}$	40.0	R$\bar{3}$	32.5
1	P$\bar{3}$c	33.3	P$\bar{3}$c	25.0

Table 3.1 can be used to determine at which points the space group transitions take place. For both series a similar pattern is found. The first transition, R$\bar{3}$c to R$\bar{3}$, takes place at $x = 0.3$. This corresponds to a M1 occupation of 80.0 % and 77.5 % for the $Ce_{(x/3)}Na_{(1-x)}Zr_2(PO_4)_3$ and $Ce_{(x/4)}Na_{(1-x)}Zr_2(PO_4)_3$ respectively. This indicates that this transition first occurs between an M1 occupancy of 80.0 to 85.0 %.

The second space group transition, from R$\bar{3}$ to P$\bar{3}$c, which is found in both end-members ($Ce_{(0.33)}Zr_2(PO_4)_3$ and $Ce_{0.25}Zr_2(PO_4)_3$) is more difficult to predict only looking at M1 occupancy. Although the M1 occupancy of $Ce_{(0.33)}Zr_2(PO_4)_3$ (33.3 %) is higher than the one for $Ce_{0.225}Na_{0.1}Zr_2(PO_4)_3$ ($x = 0.9$, 32.5 %, R$\bar{3}$), the compound still exhibits the P$\bar{3}$c space group. This indicates that a different mechanism is (mainly) responsible in this second reduction of symmetry.

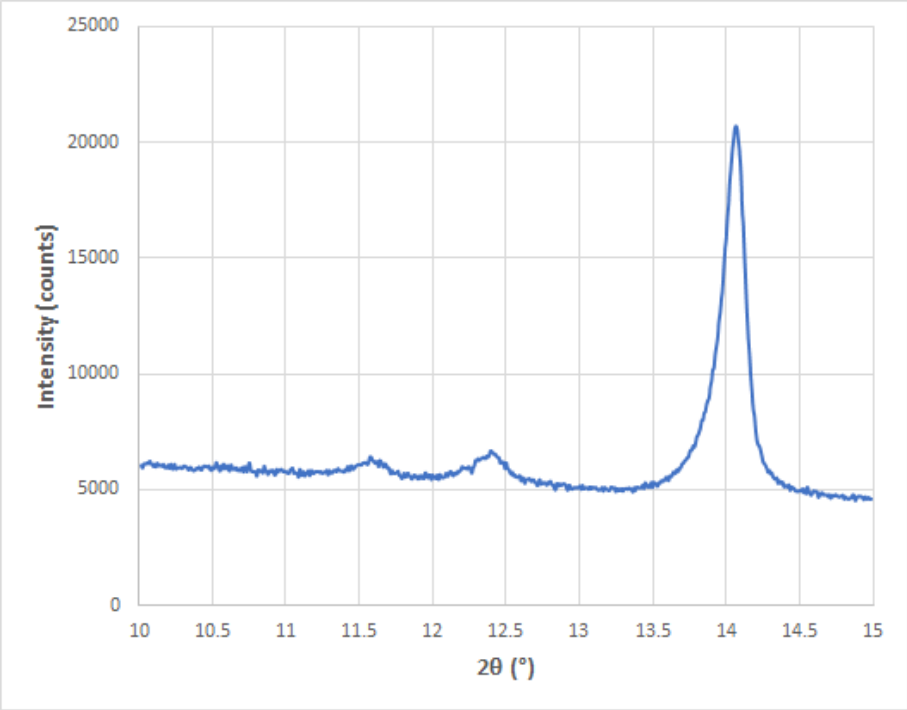

Figure 3.4: Diffractogram, 10-15 °2θ, of $Ce_{0.1}Na_{0.7}Zr_2(PO_4)_3$. The two reflections at 11.6°2θ and 12.4°2θ indicate a reduction of symmetry from $R\bar{3}c$ to $R\bar{3}$.

3.1.2. Refinement

Profile fitting

Full profile fitting and refinement was done for two end-members, $NaZr_2(PO_4)_3$ and $Ce_{0.33}Zr_2(PO_4)_3$, and for the intermediary $Ce_{0.167}Na_{0.5}Zr_2(PO_4)_3$. Considering the three different space groups present, this forms a representative base for analysis. Details of the refinements are given in Table 3.2 and the atomic positions are given in Table 3.3. Profile fitting in Fullprof [35] of the three samples can be found in Figures 3.5, 3.6 and 3.7. As the maximum reflection intensity of the two-hour $Ce_{0.33}Zr_2(PO_4)_3$ measurement was relatively low, an additional six-hour measurement was done to ensure enough data was available for a proper refinement.

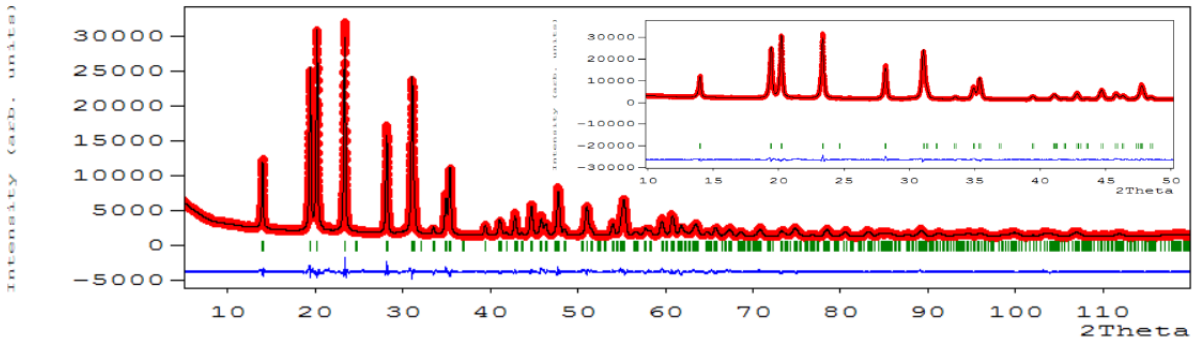

Figure 3.5: Profile fitting of $NaZr_2(PO_4)_3$ in FullProf. The red line represents the data points, whereas the black line gives the theoretical values predicted from the model. The blue line shows the difference between the data and the model. The green lines give the positions of the reflection.

Structural parameters

Profile parameters a and b were investigated using FullProf. The results are presented in Figure 3.8. For the tetravalent series only the structural parameters of the measurements in the full 5-120 °2θ range have been refined.

Table 3.2: Crystallographic data and partial results of the Rietveld refinement. R-factors are given corrected for background.

Chemical formula	$NaZr_2(PO_4)_3$	$Ce_{0.167}Na_{0.5}Zr_2(PO_4)_3$	$Ce_{0.33}Zr_2(PO_4)_3$
Structural model	$NaZr_2(PO_4)_3$ [9]	$Ca_{0.25}Sr_{0.25}Zr_2(PO_4)_3$ [36]	$Ce_{0.33}Zr_2(PO_4)_3$ [28]
Crystal system	Hexagonal	Hexagonal	Hexagonal
M1 occupation, %	100	66.7	33.3
Space group	$R\bar{3}c$ (167)	$R\bar{3}$ (148)	$P\bar{3}c$ (165)
a, *Å*	8.79274(11)	8.75477(20)	8.74191(11)
c, *Å*	22.86481(35)	22.97379(67)	23.14812(36)
V, $Å^3$	1530.799	1524.941	1531.994
Z	6	6	6
2θ-*range*, °	5-120	5-120	5-120
Number of reflections	568/2	1122/2	1634/2
General number of points	13733	13727	13727
Number of fitted parameters	11	23	81
R_B, %	2.96	8.32	6.38
R_{wp}, %	4.18	6.54	3.56
R_f, %	3.82	7.07	11.0
R_p, %	3.24	4.81	2.70
R_{exp}, %	2.14	2.22	1.33
χ^2	3.81	8.64	7.15

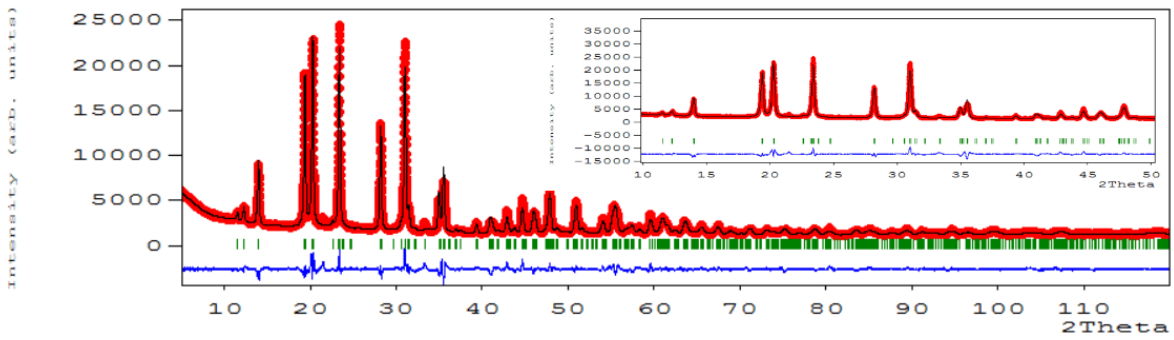

Figure 3.6: Profile fitting of $Ce_{0.167}Na_{0.5}Zr_2(PO_4)_3$ in FullProf. The red line represents the data points, whereas the black line gives the theoretical values predicted from the model. The blue line shows the difference between the data and the model. The green lines give the positions of the reflection.

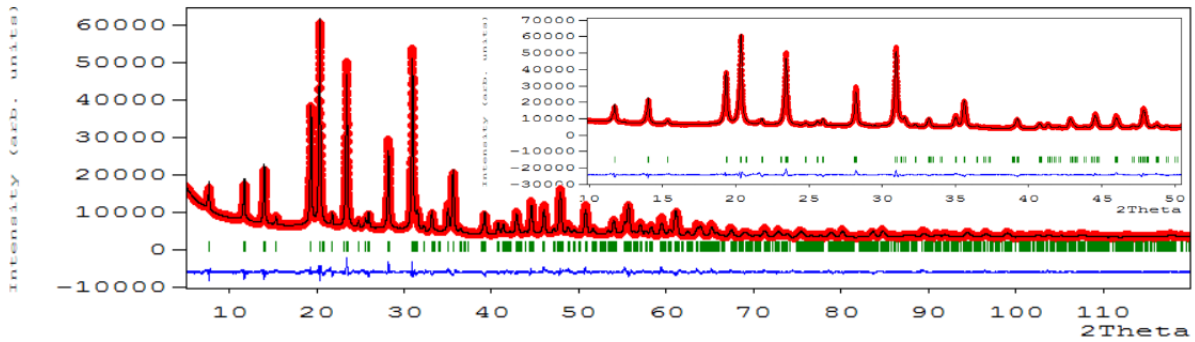

Figure 3.7: Profile fitting of $Ce_{0.33}Zr_2(PO_4)_3$ in FullProf. The red line represents the data points, whereas the black line gives the theoretical values predicted from the model. The blue line shows the difference between the data and the model. The green lines give the positions of the reflection.

In both series a shows a decrease, whereas c increases with increasing cerium content. This is in line with previous research considering the structural parameters of analogous structure types [43]. The end-members of both series, in space group $P\bar{3}c$ are an exception to the gradual increase in the value for the c parameter.

$Ce_{0.15}Na_{0.4}Zr_2(PO_4)_3$ (x=0.6, tetravalent series), shows a deviation from the average trend. Perhaps this is merely an anomaly, although it could possibly be caused by a non-random ordering of occupation of positions by the atoms within the NZP structure. This phenomenon, known as a supercell formation, has been observed in this class of materials before [44], but this cannot be proven without further transmission electroscope microscopy (TEM) analysis.

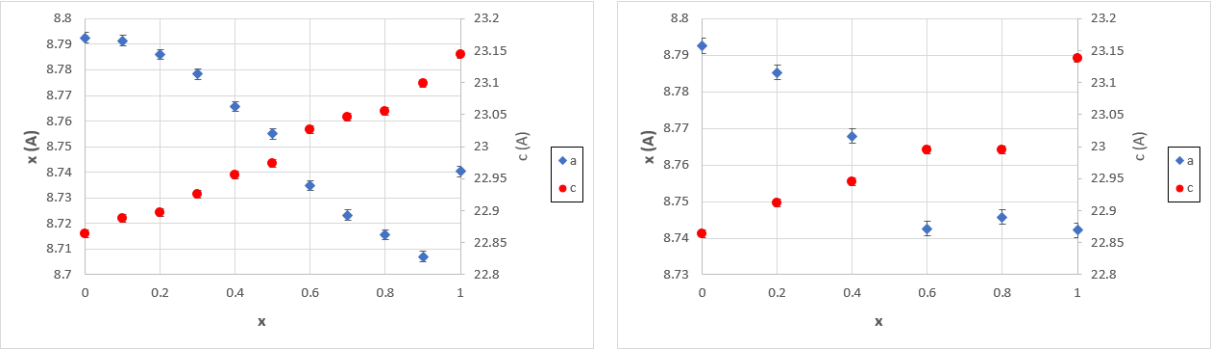

Figure 3.8: Unit cell parameters a and b variation between the different compounds of the two series (left: $Ce_{(x/3)}Na_{(1-x)}Zr_2(PO_4)_3$, right: $Ce_{(x/4)}Na_{(1-x)}Zr_2(PO_4)_3$ series). Error bars give the indicated error as taken from FullProf.

Refined atomic coordinates are presented in Table 3.3. The differences between the structural models used is reflected in the increasing complexity and number of atomic positions needed.

The structure fragments (Figure 3.9) show the increased rotation of the polyhedra with increased cerium content. The values for the interatomic distances in the three samples which have been refined are given in Table 3.4. These values correspond to the trend for a and c, as an increase in the distance Na/Ce-Zr1 results in an increase in c, whereas the decrease in the distances Na/Ce-P1, Na/Ce-O1 and Na/Ce-O2 result in a decrease in a. Again, it can be seen that the Na/Ce-P1 and Na/Ce-O1 distances increase in the end-member $Ce_{0.33}Zr_2(PO_4)_3$, resulting in the higher a value.

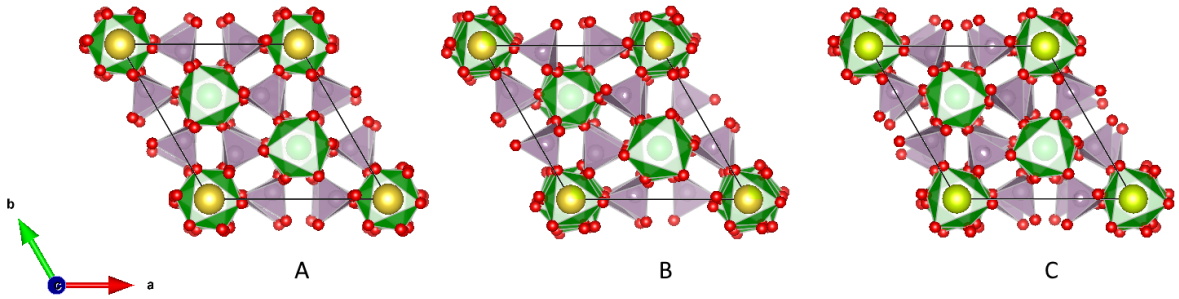

Figure 3.9: VESTA [12] renderings of three NZP structures. The green polyhedra represent the ZrO_6 octahedra with a zirconium atom in its center while the purple ones represent the PO_4 tetrahedra. Oxygen is shown in red and sodium and cerium atoms are respectively shown in yellow and light green. A: $NaZr_2(PO_4)_3$, space group $R\bar{3}c$. B: $Ce_{0.167}Na_{0.5}Zr_2(PO_4)_3$, space group $R\bar{3}$. C: $Ce_{0.33}Zr_2(PO_4)_3$, space group $P\bar{3}c$.

Table 3.3: Refined atomic positions.

$NaZr_2(PO_4)_3$					
Atom	Site	x	y	z	Occupancy
Na	$6b$	0	0	0	0.167
Zr	$12c$	0	0	0.14585(2)	0.333
P	$18e$	0.28958(14)	0	0.25	0.5
O1	$36f$	0.18486(23)	-0.01958(26)	0.19562(9)	1.0
O2	$36f$	0.19400(19)	0.16807(21)	0.08820(8)	1.0
$Ce_{0.167}Na_{0.5}Zr_2(PO_4)_3$					
Atom	Site	x	y	z	Occupancy
Ce	$3a$	0	0	0	0.028
Na	$3a$	0	0	0	0.083
Zr1	$6c$	0	0	0.14779(14)	0.333
Zr2	$6c$	0	0	0.64504(12)	0.333
P	$18f$	0.30021(57)	0.01034(83)	0.25781(23)	1.0
O1	$18f$	0.15669(126)	-0.00524(138)	0.19290(36)	1.0
O2	$18f$	0.04661(133)	-0.17553(128)	0.69602(40)	1.0
O3	$18f$	0.18889(135)	0.17081(135)	0.08049(35)	1.0
O4	$18f$	-0.17996(148)	-0.19840(131)	0.58426(39)	1.0
$Ce_{0.33}Zr_2(PO_4)_3$					
Atom	Site	x	y	z	Occupancy
Ce	$2b$	0	0	0	0.167
Zr1	$4c$	0	0	0.15092(7)	0.333
Zr2	$4d$	0.667	0.333	0.47374(9)	0.333
Zr3	$4d$	0.333	0.667	0.81630(11)	0.333
P1	$6f$	0.29520(64)	0	0.25	0.5
P2	$12g$	0.95431(44)	0.33984(62)	0.58463(20)	1.0
O1	$12g$	0.16121(112)	-0.02663(158)	0.20672(29)	1.0
O2	$12g$	0.83541(106)	0.28457(118)	0.52243(44)	1.0
O3	$12g$	0.50601(120)	0.63818(172)	0.86470(40)	1.0
O4	$12g$	0.21495(109)	0.18451(106)	0.08850(41)	1.0
O5	$12g$	0.86384(96)	0.48694(114)	0.41969(43)	1.0
O6	$12g$	0.54032(81)	0.83174(105)	0.76235(40)	1.0

Table 3.4: Selected interatomic distances as determined by Fullprof [35]. Atom 2 is indicated according to the standard NZP model. To avoid ambiguity about variation between individual models, the nearest option possible has been selected for the two remaining models.

		Distance, Å		
Atom 1	Atom 2	$NaZr_2(PO_4)_3$	$Ce_{0.167}Na_{0.5}Zr_2(PO_4)_3$	$Ce_{0.33}Zr_2(PO_4)_3$
Na/Ce	Zr1	2×3.33485(6)	2×3.39512(10)	2×3.49814(6)
Na/Ce	P1	6×3.67374(4)	6×3.49668(7)	6×3.75258(4)
Na/Ce	O1	6×4.79142(7)	6×4.64588(13)	6×4.97307(5)
Na/Ce	O2	6×2.57678(3)	6×2.43249(5)	6×2.69927(3)

3.1.3. Thermal stability

Additional measurements were done on samples of the $Ce_{(x/3)}Na_{(1-x)}Zr_2(PO_4)_3$ series after heating at 1000 °C for 24 hours to get an indication of the thermal stability of the materials. To obtain information about the decomposition of the NZP compounds a comparison has been made with the samples after heating at 800 °C. At 1000 °, the expectation is a partial decomposition of the NZP compound to primarily ZrP_2O_7, with minor constituents ZrO_2, α- and β-$Zr_2P_2O_9$ ([45], [46]). $Ce(PO_4)_3$ and $NaPO_4$ can be expected as well after decomposition ([46], [47]). To this extent the main reflection caused by the ZrP_2O_7 phase (21.5 °2θ), relative to the reflection with the highest intensity (23.4 °2θ) are compared. In theory, as the compounds decompose, the ZrP_2O_7 phase starts appearing more dominantly in the diffractograms [48].

A visual comparison of the diffractograms of $Ce_{0.033}Na_{0.9}Zr_2(PO_4)_3$, $Ce_{0.167}Na_{0.5}Zr_2(PO_4)_3$ and $Ce_{0.33}Zr_2(PO_4)_3$ is given in Figure 3.10. Results of the entire series are tabulated and are given in Table 3.5. The difference (Δ), relative to the value found at 800 °C, is also given for each compound.

Interestingly, the higher temperature caused an increase in the impurity in all samples, except for two samples with a low cerium content, which showed no sign of impurities at 800 °C ($NaZr_2(PO_4)_3$ and $Ce_{0.067}Na_{0.8}Zr_2(PO_4)_3$). The decrease of thermal stability follows an unpredictable pattern. However, samples with a high loading seem more susceptible to heating than samples with a low loading and after the 1000 °C treatment, $Ce_{0.267}Na_{0.2}Zr_2(PO_4)_3$ has a detectable impurity, even though this was not apparent at 800 °C.

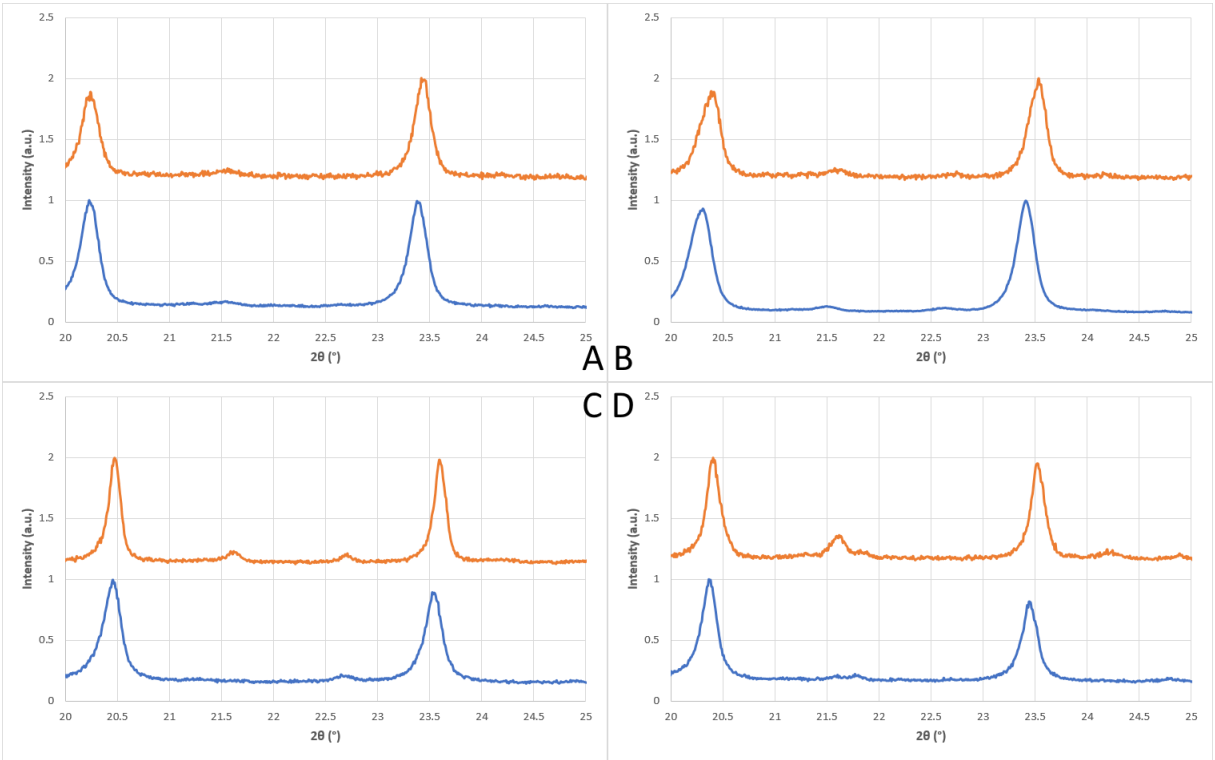

Figure 3.10: A visual comparison of the diffractograms of $Ce_{0.033}Na_{0.9}Zr_2(PO_4)_3$ (A), $Ce_{0.167}Na_{0.5}Zr_2(PO_4)_3$ (B), $Ce_{0.267}Na_{0.2}Zr_2(PO_4)_3$ (C) and $Ce_{0.33}Zr_2(PO_4)_3$ (D) at 800 °C and 1000 °C. 1000 °C measurements were done using a cobalt tube, results have been adjusted by 2θ shift in Fullprof to ease comparison with the copper tube measurements. Blue represents data for 800 °C and orange represents data for 1000 °C.

Table 3.5: Comparison of relative intensities of the main phase (NZP), a peak hkl of 113, and the impurity (ZrP_2O_7), a peak hkl of 200, at 800 °C and 1000 °C.

	$I_{ZrP_2O_7}/I_{NZP}$		
Compound	800 °C	1000 °C	Δ (+%)
$NaZr_2(PO_4)_3$	0	0	-
$Ce_{0.033}Na_{0.9}Zr_2(PO_4)_3$	0.047	0.13	180
$Ce_{0.067}Na_{0.8}Zr_2(PO_4)_3$	0	0	-
$Ce_{0.1}Na_{0.7}Zr_2(PO_4)_3$	0.039	0.10	160
$Ce_{0.133}Na_{0.6}Zr_2(PO_4)_3$	0.035	0.090	158
$Ce_{0.167}Na_{0.5}Zr_2(PO_4)_3$	0.040	0.073	79.5
$Ce_{0.2}Na_{0.4}Zr_2(PO_4)_3$	0.036	0.11	216
$Ce_{0.233}Na_{0.3}Zr_2(PO_4)_3$	0.035	0.078	125
$Ce_{0.267}Na_{0.2}Zr_2(PO_4)_3$	0	0.10	-
$Ce_{0.3}Na_{0.1}Zr_2(PO_4)_3$	0.042	0.15	261
$Ce_{0.33}Zr_2(PO_4)_3$	0.042	0.23	443

3.2. SEM

Pure NZP and four members ($x = 0.3, 0.5, 0.9, 1.0$) of the trivalent series have been examined by scanning electron microscopy. Results of these measurements are presented in Figure 3.12. The difference between the end-member ($x = 1.0$) and the other synthesized compounds is striking, due to a distinct difference in particle size (Figure 3.11), although the method of preparation is identical.

In general, particle surfaces appear smooth. Particle size is, however, not homogeneous as even within one sample, notable differences in size can be observed. This might be due to the method of manual grinding the compounds. Values of 30 to 70 nm can be found in literature for average crystallite size for NZP-type compounds. This is in line with the smaller particles observed on the SEM images ([49], [50]). This is also an indication that further grinding would possibly improve the crystallinity of the compounds as the larger particles analyzed are in the order of ~20 μm.

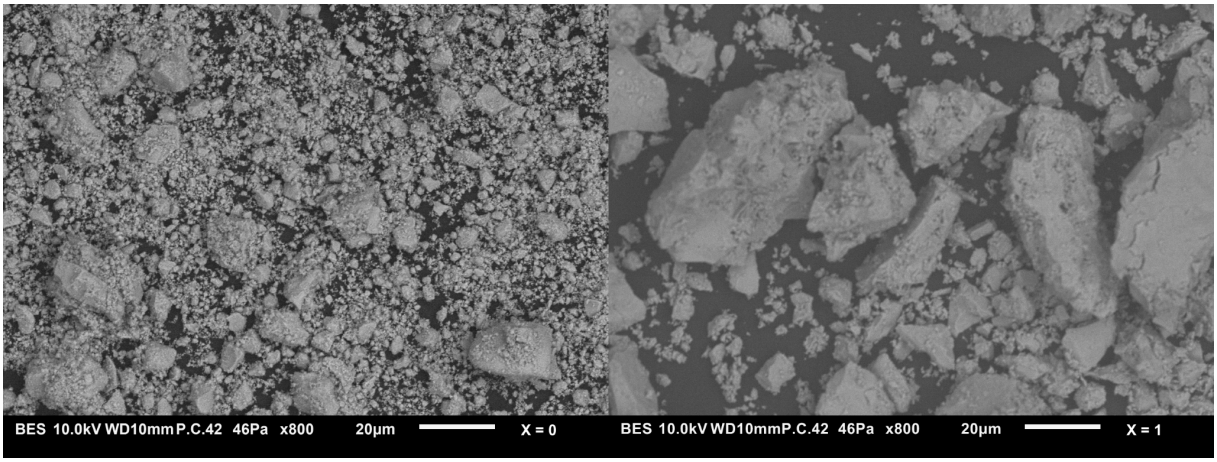

Figure 3.11: SEM images of two selected samples (left: $NaZr_2(PO_4)_3$, right: $Ce_{0.33}Zr_2(PO_4)_3$).

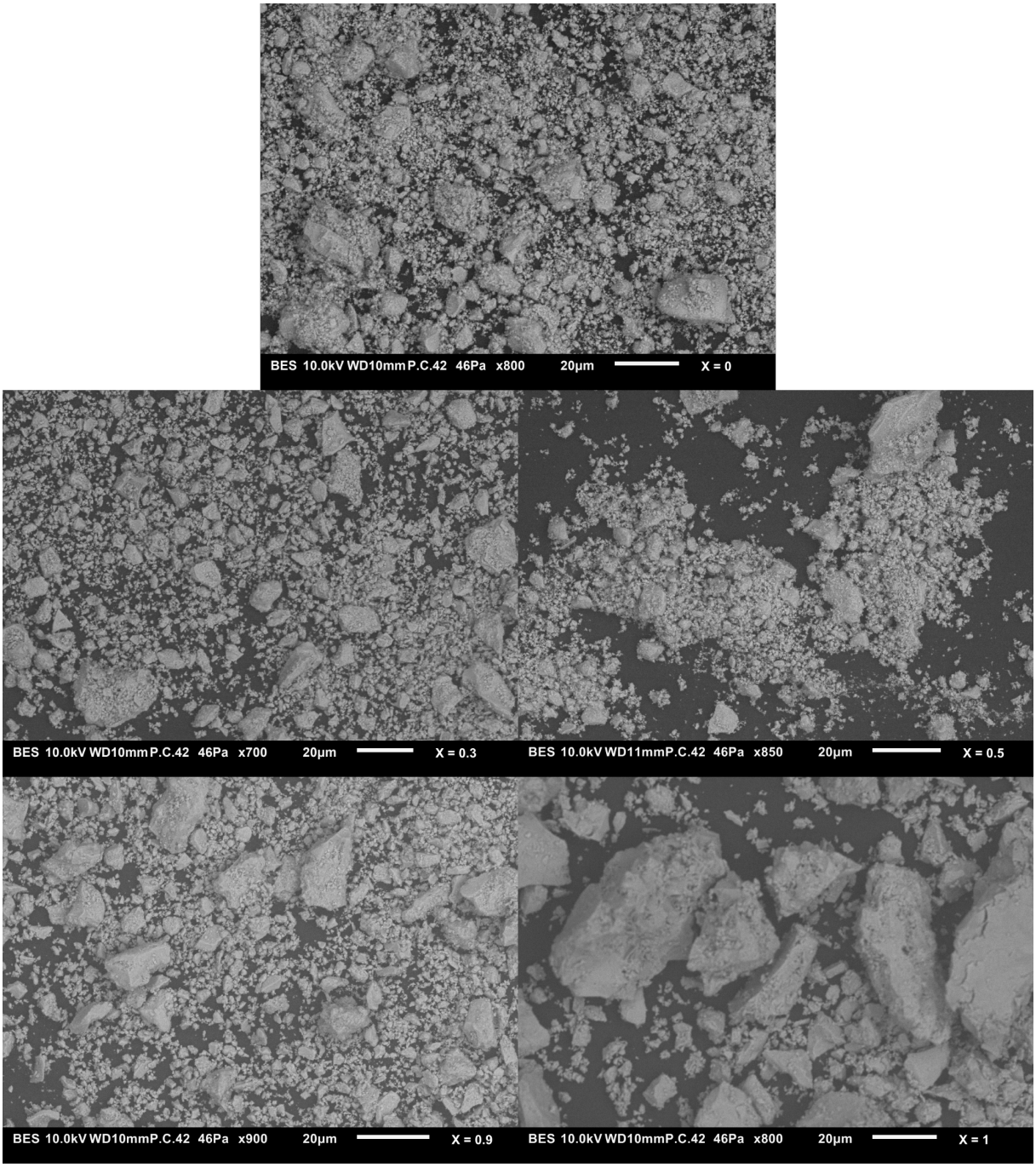

Figure 3.12: SEM images of pure NZP (on top) and four selected samples from the $Ce_{(x/3)}Na_{(1-x)}Zr_2(PO_4)_3$ series, cerium loading is indicated on the bottom right corner of every image.

3.3. IR-spectroscopy

IR-spectra have been recorded for pure NZP, five members ($x = 0.2, 0.4, 0.6, 0.8, 1.0$) of the $Ce_{(x/3)}Na_{(1-x)}Zr_2(PO_4)_3$ series and four members ($x = 0.3, 0.5, 0.9, 1.0$) of the $Ce_{(x/4)}Na_{(1-x)}Zr_2(PO_4)_3$ series. The results of these measurements, in the range of 300 to 1300 cm^{-1}, are given in Figure 3.13. Four areas of interest can be identified.

In the IR spectrum of $NaZr_2(PO_4)_3$ an intense broad band at 1030 cm^{-1} including the shoulder just above 1200 cm^{-1}, a result of asymmetric stretching vibrations v_3 of the P-O bond in the PO_4 tetrahedron, a band in the 540 to 630 cm^{-1}, a result of the bending vibrations v_4 and a band around 400 cm^{-1}, a result of the bending vibrations v_2 of the PO_4 tetrahedron can be observed, in line with tabulated values ([51], [52]). When more cerium is present in the compound the symmetric stretching vibration v_1 of the P-O bond around 930 cm^{-1} becomes more distinct.

In general, the IR spectra for both series show striking similarity. This shows that all compounds belong to the same orthophosphate class. Some differences can, however, be seen. While the end-members $Ce_{0.33}Zr_2(PO_4)_3$ and $Ce_{0.33}Zr_2(PO_4)_3$ show similarity to comparable compounds in the $P\bar{3}c$ space group [52], it is observed that the peaks of the broad band related to the asymmetric stretching vibrations splits into more well-defined peaks with an increasing value of x. This is in line with expectations, as the number of theoretical bands increases in the space group transition of $R\bar{3}c$ to $R\bar{3}$ [53]. A comparison of the indexed peaks and values found in literature is given in Table 3.6.

Table 3.6: Comparison of the IR-spectroscopy data found in the current work to values found in literature ([51], [52], [53]).

	$NaZr_2(PO_4)_3$		**$Ce_{0.33}Zr_2(PO_4)_3$**		**$Ce_{0.25}Zr_2(PO_4)_3$**
Type of vibration	*Literature*	*Current work*	*Literature*	*Current work*	*Current work*
v_3	1200 1045-1030	1205 1045	1280 1155 1125 1105 1080 1060 1045 1020	- 1164 - 1096 - 1053 1040 1012	- 1155 - 1105 - 1055 1040 1012
v_1			980 945 935	974 - 928	976 - 930
v_4	640-630 - 555	645 575 555	645 560-540	632 552	634 552 517
v_2	420 <400	418 385 360	440 <400	430 355	420 362

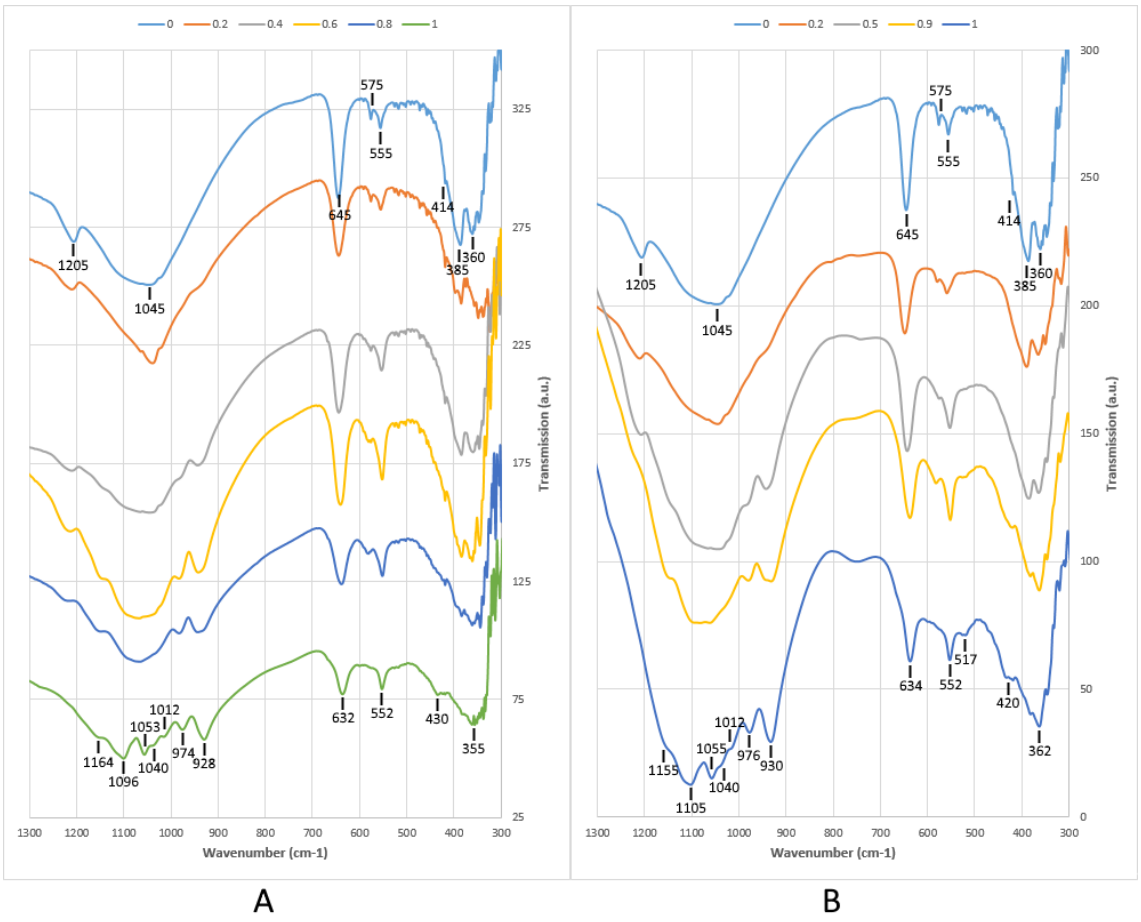

Figure 3.13: A: IR-spectra of five selected samples from the trivalent ($Ce_{(x/3)}Na_{(1-x)}Zr_2(PO_4)_3$) series. Peak positions are given for the two end-members. B: IR-spectra of four selected samples from the tetravalent ($Ce_{(x/4)}Na_{(1-x)}Zr_2(PO_4)_3$) series. Peak positions are given for the two end-members.

4

Conclusion

The current work indicates the potential of using NZP-type ceramics for storage of plutonium waste. Two series, $Ce_{(x/3)}Na_{(1-x)}Zr_2(PO_4)_3$ and $Ce_{(x/4)}Na_{(1-x)}Zr_2(PO_4)_3$, have been successfully synthesized using solid-state preparation methods, in which cerium was used as a plutonium analogue. The characteristics of the compounds have been determined using XRD, SEM and IR-spectroscopy.

Interestingly, greater insight has been found for the space group transition from $R\bar{3}c$ to $P\bar{3}c$, as members of both series for $0.3 \leq x \leq 0.9$ have been found to exhibit the $R\bar{3}$ space group. For $x < 0.3$ the space group $R\bar{3}c$ has been found, in accordance with the end-member $NaZr_2(PO_4)_3$. For $x = 1$, the space group $P\bar{3}c$ was found, which is similar to literature.

Using Rietveld refinement, profile parameters for both series were determined. Both series followed a similar trend, in which the a parameter decreased when more cerium was introduced, whereas the c parameter followed the opposite trend. Furthermore, the XRD analysis on samples with different heat treatments (800 °C and 1000 °C), indicates that an increase in cerium content negatively influences the stability of the NZP phase. However, this phase is still dominant for all compounds analyzed up to at least 1000 °C. Besides this trend in thermal stability, a decrease in stability can be detected by the increased distortion of the polyhedra in the NZP crystal structure, which induces a less-ordered structure. SEM analysis has given information about the difference in morphology between members of the $Ce_{(x/3)}Na_{(1-x)}Zr_2(PO_4)_3$ series. The SEM pictures show a clear deviation in structure for the end-member $Ce_{0.33}Zr_2(PO_4)_3$, but the reason for this anomaly is not entirely clear. Furthermore, this analysis gave the indication that the synthesis method could be sub-optimal and improvements can be made in the future. The IR-spectra indicate that all compounds measured belong to the same orthophosphate class and bands are visible in expected positions, according to the space group transitions.

Both the XRD and IR-spectroscopy results show a high similarity between the two series. Therefore, the most intriguing question which remains is whether the oxidation states of cerium in the synthesized NZP compounds are indeed 3+ and 4+, as was intended.

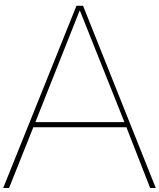

Acknowledgements

This bachelor thesis could not have been done without any external help. First and foremost, I would like to thank the research group Reactor Physics and Nuclear Materials, for providing me with this opportunity as well as a warm welcome and Denis Bykov in particular for his supervision during this project. Furthermore, I would like to thank Kees Goubitz for his help and advise concerning the XRD machine and Andrea Sabau for her assistance with the SEM machine.

B

Future research

More characteristics of the synthesized compounds can still be examined. This is a possible starting point for a follow-up research. Firstly, a leaching test should be done to determine the leaching rates for samples from both series, as this is an important parameter for the storage of the nuclear waste and gives insights in the chemical stability of the waste matrix. Secondly, X-ray photoelectron spectroscopy (XPS) analysis should be carried out to determine if the cerium actually stays in the wanted oxidation state using the current experimental approach, as this is critical for predicting the behaviour of plutonium in the waste matrix. Lastly, thermogravimetric (TGA) analysis could provide a better understanding of the thermal stability of the synthesized materials.

Bibliography

[1] International Atomic Energy Agency. Storage and Disposal of Spent Fuel and High Level Radioactive Waste. *IAEA Policy*, 2006.

[2] E. H. Oelkers and J. M. Montel. Phosphates and Nuclear Waste Storage. *Elements*, 4: 113–116, 2008.

[3] S. Panja. Studies on the transport behavior of actinides and lanthanides across supported liquid membranes containing Di Glycoamide carriers. *(Thesis, Mumbai)*.

[4] R. Naudet. The Oklo Phenomenon. *IAEA-Symposium*, 1975.

[5] V. I. Pet'kov, E. A. Asabina, M. V. Sukhanov, I. A. Schelokov, A. S. Shipilov, and A. A. Alekseev. Design and Characterization of Phosphate-Containing Ceramics with Kosnarite- and Langbeinite-Type Structures for Industrial Applications. *Chemical Engineering Transactions*, 43:1825–1830, 2015.

[6] B. E. Scheetz, D. K. Agrawal, E. Breval, and R. Roy. Sodium Zirconium Phosphate (NZP) as a host structure for nuclear waste immobilization: A Review. *Waste Management*, 14:489–505, 1994.

[7] I. A. Orlova, D. B. Kitaev, A. N. Lukinich, S. B. Tomilin, A. A. Lizin, I. A. Kulikov, and V. E. Samsonov. Phosphate monazite- and NaZr2(PO4)3 (NZP)-like ceramics containing uranium and plutonium. *Czechoslovak Journal of Physics*, 53, 2003.

[8] M. Numata, S. Mihara, S. Kojima, H. Ito, and T. Kato. Reduction of Sodium Nitrate Liquid Waste in Nuclear Reprocessing Plants. *WM Conference*, pages 1–8, 2006.

[9] L. O. Hagman and P. Kierkegaard. The Crystal Structure of NaMe2(IV)(PO4)3; Me(IV) = Ge, Ti, Zr. *Acta Chemica Scandinavica*, 22:1822–1832, 1968.

[10] V. I. Pet'kov, E. A. Asabina, and I. A. Schelokov. Thermal Expansion of NASICON Materials. *Inorganic Materials*, 49:502–506, 2013.

[11] H. T. Hawkins, D. R. Spearing, D. K. Veirs, J. A. Danis, D. M. Smith, C. D. Tait, and W. H. Runde. Synthesis and Characterization of Uranium(IV)-Bearing Members of the [NZP] Structural Family. *Chemical Materials*, 11:2851–2857, 1999.

[12] K. Momma and F. Izumi. VESTA: a three-dimensional visualization system for electronic and structural analysis. *Journal of Applied Crystallography*, 41:653–658, 2008.

[13] V. I. Pet'kov and A. I. Orlova. Crystal-Chemical Approach to Predicting the Thermal Expansion of Compounds in the NZP Family. *Inorganic Materials*, 39:1013–1023, 2003.

[14] V. I. Pet'kov, A. I. Orlova, and G. N. Kasantsev. Thermal Expansion in the Zr and 1-, 2-Valent Complex Phosphates of NaZr2(PO4)3 (NZP) Structure. *Journal of Thermal Analysis and Calorimetry*, 66:623–632, 2001.

[15] M. I. Ojovan and O. G. Batyukhnova. Glasses for Nuclear Waste Immobilization. *WM Conference*, 2007.

[16] U. Ahmadu, A. O. Musa, S. A. Jonah, and N. Rabiu. Synthesis and thermal characterization of NZP compounds Na1-xLixZr2(PO4)2 (x = 0.00-0.75). *Journal of Thermal Analysis and Calorimetry*, 101:175–179, 2010.

[17] L. M. van Koppen. NZP-type ceramics for simultaneous incorporation of radioisotopes of cesium strontium and minor actinides. *(Thesis, TU Delft)*, 2015.

[18] A. Bohre and K. Awasthi. Immobolization of radioactive waste in ceramic based hosts. *Anchor Academic Publishing*, pages 14–16, 2014.

[19] D. M. Bykov, A. I. Orlova, S. V. Tomilin, A. A. Lizin, and A. N. Lukinykh. Americium and Plutonium in Trigonal Phosphates (NZP Type) Am1/3[Zr2(PO4)3] and Pu1/4[Zr2(PO4)3]. *Radiochemistry*, 48:234–239, 2006.

[20] A. Kanunov, B. Glorieux, A. Orlova, E. Borovikova, and G. Zavedeeva. Synthesis, Structure and Luminescence Properties of Phosphates A(1-3x)Eu(x)Zr2(PO4)3 (A – Alkali Metal). *Manuscript*, pages 1–16, 2016.

[21] O. Selinus. Perspectives and Prospects. *Essentials of Medical Geology (Publisher: Elsevier Academic Press)*, 1:4–6, 2005.

[22] Y. Miyajima, Y. Saito, M. Matsuoka, and Y. Yamamoto. Ionic conductivity of NASICON-type Na1+xMxZr2-xP3O12 (M: Yb, Er, Dy). *Solid State Ionics*, 84:61–64, 1996.

[23] A. I. Orlova. Isomorphism in Crystalline Phosphates of the NaZr2(PO4)3 Structural Type and Radiochemical Problems. *Radiochemistry*, 44:423–445, 2002.

[24] S. Le Solliec, A. J. Popel, and I. Farnan. Cerium dioxide as a proxy for Uranium dioxide. *Ecole Nationale Superieure de Chimie de Clermont-Ferrand*, 2013.

[25] R. D. Shannon. Revised Effective Ionic Radii and Systematic Studies of Interatomic Distances in Halides and Chalcogenides. *Acta Crystallographica*, 32:751–767, 1976.

[26] N. A. Chapman and J. A. T. Smellie. Introduction and summary of the workshop: Natural analogues to the conditions around a final repository for high-level radioactive waste. *Chemical Geology*, 55:167–173, 1986.

[27] Department of Energy, National Nuclear Security Administration. Surplus Plutonium Disposition Program. *Federal Register*, 67:19432–19435, 2002.

[28] D. M. Bykov, E. R. Gobechiya, Y. K. Kabalov, A. I. Orlova, and S. V. Tomilin. Crystal structures of lanthanide and zirconium phosphates with general formula Ln0.33Zr2(PO4)3, where Ln = Ce, Eu, Yb. *Journal of Solid State Chemistry*, 179:3101–3106, 2006.

[29] J. V. Bothe and P. W. Brown. Low Temperature Synthesis of Porous NZP Ceramics. *Journal of the American Ceramic Society*, 91:2059–2063, 2008.

[30] D. K. Agrawal, C. Y. Huang, and H. A. McKinstry. NZP: A New Family of Low-Thermal Expansion Materials. *International Journal of Thermophysics*, 12:697–710, 1991.

[31] M. Sugantha, U. V. Varadaraju, and G. V. Subba Rao. Synthesis and Characterization of NZP Phases AM'3+M"4+P3O12. *Journal of Solid State Chemistry*, 111:33–40, 1994.

[32] A. M. Ross, M. N. Williams, D. R. Talham, and J. J. Keaffaber. Zirconium Phosphate and Phosphonate Nanoparticles for Phosphate Removal from Water: An Aquarium Life Support System Application. *Manuscript*, 2010.

[33] A. Chauhan and P. Chauhan. Powder XRD Technique and its Applications in Science and Technology. *Journal of Analytical and Bioanalytical Techniques*, 5, 2014.

[34] T. Degen, M. Sadki, E. Bron, U. König, and G. Nénert. The HighScore suite. *Powder Diffraction*, 29 (S2):S13–S18, 2014.

[35] J. Rodriguez-Carvajal. Fullprof: A Program for Rietveld Refinement and Pattern Matching Analysis. *Abstract of the Satellite Meeting on Powder Diffraction of the XV Congress of the IUCr, Toulouse, France*, page 127, 1990.

[36] D. A. Woodcock, P. Lightfoot, and R. I. Smith. Powder neutron diffraction studies of three low thermal expansion phases in the NZP family: K0.5Nb0.5Ti1.5(PO4)3, Ba0.5Ti2(PO4)3 and Ca0.25Sr0.25Ti2(PO4)3. *Journal of Materials Chemistry*, 9:2631–2636, 1999.

[37] J. Goldstein, D. E. Newbury, P. Echlin, D. C. Joy, A. D. Romig Jr, C. E. Lyman, C. Fiori, and E. Lifshin. Scanning Electron Microscopy and X-Ray Microanalysis: A Text for Biologists, Material Scientists, and Geologists. *Plenum Press*, 2:1–20, 1992.

[38] B. Stuart. Infrared Spectroscopy: Fundamentals and Applications. *Analytical Techniques in the Sciences*, pages 1–2, 2004.

[39] L. Berzina-Cimdina and N. Borodajenko. Infrared Spectroscopy - Materials Science, Engineering and Technology. *Intech*, pages 123–147, 2012.

[40] V. S. Kurazhkovskaya, D. M. Bykov, E. Yu. Borovikova, N. Yu. Boldyrev, L. Mikhalitsyn, and A. I. Orlova. Vibrational spectra and factor group analysis of lanthanide and zirconium phosphates M(III) 0.33Zr2(PO4)3, where M(III) = Y, La–Lu. *Vibrational Spectroscopy*, 52:137–143, 2010.

[41] M. Orlova, L. Perfler, M. Tribus, P. Salnikov, B. Glorieux, and A. Orlova. Temperature induced phase transition of CaMn0.5Zr1.5(PO4)3 phosphate. *Journal of Solid State Chemistry*, 235:36–42, 2016.

[42] M. Barre, M. P. Crosnier-Lopez, F. Le Berre, J. Emery, E. Suard, and J. L. Fourquet. Room Temperature Crystal Structure of La1/3Zr2(PO4)3, a NASICON-type Compound. *Chemical Materials*, 17:6605–6610, 2005.

[43] S. N. Achary, O. D. Jayakumar, S. J. Patwe, A. B. Shinde, P. S. R. Krishna, S. K. Kulshreshta, and A. K. Tyagi. Neutron diffraction studies on Ca1−xBaxZr4P6O24 solid solutions. *Pramana - journal of physics*, 71:941–946, 2008.

[44] M. Barré, M. P. Crosnier-Lopez, F. Le Berre, O. Bohnké, E. Suard, and J. L. Fourquet. Double NASICON-type cell: ordered Nd3+ distribution in Li0.2Nd0.8/3Zr2(PO4)3. *Dalton Transactions*, pages 3061–3069, 2008.

[45] A. Clearfield, R. Querra, A. Oskarsson, M. A. Subramanian, and W. Wang. Preparation of Sodium Zirconium Phosphates of the Type Na1+4xZr2-x(PO4)3. *Materials Research Bulletin*, 18:1561–1567, 1983.

[46] J. M. Heintz, L. Rabardel, M. Al Qaraoui, M. Alami Talbi, R. Brochu, and G. Le Flem. New low thermal expansion ceramics: Sintering and thermal behavior of Ln1/3Zr2(PO4)3-based composites. *Journal of Alloys and Compounds*, 250:515–519, 1997.

[47] A. I. Orlova, S. G. Samoilov, G. N. Kazantsev, V. Yu. Volgutov, and A. Yu. Kazakova. Erbium Zirconium Phosphate Er0.33Zr2(PO4)3 of the NaZr2(PO4)3 Family. Structure Contraction on Heating. *Radiochemistry*, 52:666–669, 2010.

[48] D. M. Bykov, R. J. M. Konings, C. Apostolidis, A. Hen, E. Colineau, T. Wiss, and P. Raison. Synthesis and investigation of neptunium zirconium phosphate, a member of the NZP family: crystal structure, thermal behaviour and Mössbauer spectroscopy. *Manuscript*, 2017.

[49] A. I. Orlova, A. E. Kanunov, E. N. Gorshkova, A. N. Shushunov, S. N. Pleskova, E. R. Mikheeva, D. O. Savinykh, and E.S. Leonov. Synthesis, Luminescence, and Biocompatibility of Calcium and LanthanideContaining NaZr2(PO4)3Type Compounds. *Inorganic Materials*, 49:89–94, 2013.

[50] R. Velchurri, B. V. Kumar, V. R. Devi, S. I. Seok, and M. Vithal. Low temperature preparation of NaTi2(PO4)3 by sol-gel method. *International Journal of Nanotechnology*, 7:1077–1086, 2010.

[51] V. S. Kurazhkovskaya, A. I. Orlova, V. I. Petkov, D. V. Kemenov, and L. N. Kaplunnik. IR Study of the Structure of Rhombohedral Zirconium and Alkali Metal Orthophosphates. *Journal of Structural Chemistry*, 41:61–66, 2000.

[52] E. Y. Borovikova, V. S. Kurazhkovskaya, D. M. Bykov, and A. I. Orlova. Infrared Spectroscopy and the Structure of La0.33Zr2(PO4)3-Yb0.33Zr2(PO4)3 Solid Solutions. *Journal of Structural Chemistry*, 51:40–44, 2010.

[53] V. S. Kurazhkovskaya, D. M. Bykov, and A. I. Orlova. Infrared Spectroscopy and the Structure of Trigonal Zirconium Orthoposphates with Lanthanides and Actinides. *Journal of Structural Chemistry*, 45:966–971, 2004.